Tuned Responses of Astrocytes and Their Influence on Hemodynamic Signals in the Visual Cortex

James Schummers, *et al.*

Science **320**, 1638 (2008);
DOI: 10.1126/science.1156120

Science (print ISSN 0036-8075; online ISSN 1095-9203) is published weekly, except the last week in December, by the American Association for the Advancement of Science, 1200 New York Avenue NW, Washington, DC 20005.

duced for EpsE or lacking *motA* and *motB* was consistent with a calculated root mean square angular deviation of ~80° in 90 s for a *B. subtilis* cell tethered by an unpowered flagellum freely rotating by Brownian motion (supporting online material). In contrast, the angular deviation is much less, ~3°, for an *E. coli* cell tethered by an immobilized flagellum (*22*). Thus, EpsE acted as a clutch; when EpsE was induced, the flagella behaved as though they were unpowered rather than immobilized.

The biological function of the clutch appears to be related to the *B. subtilis* biofilm because *epsE* is encoded within the 15-gene *eps* operon that promotes the biosynthesis of the biofilm EPS and is repressed by SinR, the master regulator of biofilm formation. Therefore, control of a single locus ensures that cells become immobilized concomitant with biofilm formation (fig. S5A). In wild-type cells, trapped flagella and puncta of EpsE were observed within biofilm aggregates, and the cells within the aggregates were sessile (fig. S6 and movie S5). Cells expressing the $FliG^{V338A}$ clutch-insusceptible allele formed aggregates, but the cells writhed within the confines of the matrix (movie S6). We hypothesize that the clutch helps to stabilize biofilms in the environment and acts as a fail-safe mechanism to ensure that flagella do not rotate while the cells are bound by EPS.

The bacterial flagellum, powered by a motor that generates 1400 pN-nm of torque, can rotate at a frequency of greater than 100 Hz (*23*). EpsE disabled this powerful biological motor when associated with a flagellar basal body and, in a manner similar to that of a clutch, disengaged the drive train from the power source (fig. S5B). Clutch control of flagellar function has distinct advantages over transcriptional control of flagellar gene expression for regulating motility. Some bacteria, such as *E. coli* and *B. subtilis*, have many flagella per cell. The flagellum is an elaborate, durable, energetically expensive, molecular machine and simply turning off de novo flagellum synthesis does not necessarily arrest motility. Once flagellar gene expression is inactivated, multiple rounds of cell division may be required to segregate preexisting flagella to extinction in daughter cells. In contrast, the clutch requires the synthesis of only a single protein to inhibit motility. Furthermore, if biofilm formation is prematurely aborted, flagella once disabled by the clutch might be reactivated, allowing cells to bypass fresh investment in flagellar synthesis. Whereas flagellum expression and assembly are complex and slow, clutch control is simple, rapid, and potentially reversible.

References and Notes

1. R. Kolter, P. Greenberg, *Nature* **441**, 300 (2006).
2. R. M. Macnab, *Annu. Rev. Microbiol.* **57**, 77 (2003).
3. H. C. Berg, *Annu. Rev. Biochem.* **72**, 19 (2003).
4. S. S. Branda, S. Vik, L. Friedman, R. Kolter, *Trends Microbiol.* **13**, 20 (2005).
5. D. B. Kearns, F. Chu, S. S. Branda, R. Kolter, R. Losick, *Mol. Microbiol.* **55**, 739 (2005).
6. S. S. Branda, J. E. González-Pastor, S. Ben-Yehuda, R. Losick, R. Kolter, *Proc. Natl. Acad. Sci. U.S.A.* **98**, 11621 (2001).
7. F. Chu, D. B. Kearns, S. S. Branda, R. Kolter, R. Losick, *Mol. Microbiol.* **59**, 1216 (2006).
8. E. R. LaVallie, M. L. Stahl, *J. Bacteriol.* **171**, 3085 (1989).
9. P. M. Coutinho, E. Deleury, G. J. Davies, B. Henrissat, *J. Mol. Biol.* **328**, 307 (2003).
10. C. Garinot-Schneider, A. C. Lellouch, R. A. Geremia, *J. Biol. Chem.* **275**, 31407 (2000).
11. D. F. Blair, H. C. Berg, *Cell* **60**, 439 (1990).
12. S. A. Lloyd, H. Tang, X. Wang, S. Billings, D. F. Blair, *J. Bacteriol.* **178**, 223 (1996).
13. D. R. Thomas, N. R. Francis, C. Xu, D. J. DeRosier, *J. Bacteriol.* **188**, 7039 (2006).
14. V. M. Irikura, M. Kihara, S. Yamaguchi, H. Sockett, R. M. Macnab, *J. Bacteriol.* **175**, 802 (1993).
15. S. A. Lloyd, D. F. Blair, *J. Mol. Biol.* **266**, 733 (1997).
16. D. L. Marykwas, S. A. Schmidt, H. C. Berg, *J. Mol. Biol.* **256**, 564 (1996).
17. J. Zhou, S. A. Lloyd, D. F. Blair, *Proc. Natl. Acad. Sci. U.S.A.* **95**, 6436 (1998).
18. P. N. Brown, M. Terrazas, K. Paul, D. F. Blair, *J. Bacteriol.* **189**, 305 (2007).
19. S. Kojima, D. F. Blair, *Biochemistry* **40**, 13041 (2001).
20. T. Mashimo, M. Hashimoto, S. Yamaguchi, S.-I. Aizawa, *J. Bacteriol.* **189**, 5153 (2007).
21. S. M. Block, D. F. Blair, H. C. Berg, *Nature* **338**, 514 (1989).
22. S. M. Block, D. F. Blair, H. C. Berg, *Cytometry* **12**, 492 (1991).
23. N. C. Darnton, L. Turner, S. Rojevsky, H. C. Berg, *J. Bacteriol.* **189**, 1756 (2007).
24. P. N. Brown, C. P. Hill, D. F. Blair, *EMBO J.* **21**, 3225 (2002).

25. We thank N. Darnton, G. Glekas, B. Haldenwang, A. Camp, Y. Le Breton, S. Mukhopadhyay, G. Ordal, and D. Rudner for reagents, constructs, and technical assistance. We thank S. Ben Yehuda, D. Blair, C. Fuqua, D. Higgins, P. Levin, R. Losick, S. Mukhopadhyay, and D. Rudner for insightful discussions and critical comments on the manuscript. This work was supported by NIH grant AI065540 (to H.C.B.) and NSF grant MCB-0721187 (to D.B.K.).

Supporting Online Material

www.sciencemag.org/cgi/content/full/320/5883/1636/DC1
Materials and Methods
SOM Text
Figs. S1 to S7
Tables S1 to S3
References
Movies S1 to S6

17 March 2008; accepted 22 April 2008
10.1126/science.1157877

Tuned Responses of Astrocytes and Their Influence on Hemodynamic Signals in the Visual Cortex

James Schummers,* Hongbo Yu,* Mriganka Sur†

Astrocytes have long been thought to act as a support network for neurons, with little role in information representation or processing. We used two-photon imaging of calcium signals in the ferret visual cortex in vivo to discover that astrocytes, like neurons, respond to visual stimuli, with distinct spatial receptive fields and sharp tuning to visual stimulus features including orientation and spatial frequency. The stimulus-feature preferences of astrocytes were exquisitely mapped across the cortical surface, in close register with neuronal maps. The spatially restricted stimulus-specific component of the intrinsic hemodynamic mapping signal was highly sensitive to astrocyte activation, indicating that astrocytes have a key role in coupling neuronal organization to mapping signals critical for noninvasive brain imaging. Furthermore, blocking astrocyte glutamate transporters influenced the magnitude and duration of adjacent visually driven neuronal responses.

Though astrocytes are the major class of nonneuronal cell in the brain (*1*), their role in brain function is unresolved. Evidence has accumulated for an active role of astrocytes in brain function (*1*–*3*). Astrocytes are closely apposed to many central synapses (*4*, *5*) and can respond to a number of neurotransmitters, including glutamate (*6*), by increases in intracellular calcium. In turn, astrocytes release glutamate and other neuroactive substances (*7*–*10*) that affect neuronal activity (*11*) and can modulate synaptic strength (*10*, *12*, *13*). Astrocytes contact vascular networks and can potentially influence the cerebral microcirculation (*14*–*16*), which has led to the proposal that astrocytes might support indirect, hemodynamic imaging of neuronal activity (*17*, *18*). Despite these in vitro studies, however, little is known about the behavior of astrocytes in vivo. Pioneering studies have demonstrated that astrocytes do respond to neural activity in vivo (*19*–*21*), but fundamental questions about the relationship between neuronal networks, astrocytes, and hemodynamic responses remain unsolved.

The precise orderly mapping of orientation preference in the visual cortex of higher mammals provides a model system with which to study these interactions. The synaptic input near pinwheel centers is nearly untuned (*22*), yet individual neurons are sharply tuned because of nonlinear filtering of inputs (*23*) and are organized on a scale of less than 50 μm (*24*). Do astrocyte responses passively follow the untuned

Picower Institute for Learning and Memory, Department of Brain and Cognitive Sciences, Massachusetts Institute of Technology, Cambridge, MA 02139, USA.

*These authors contributed equally to this work.
†To whom correspondence should be addressed. E-mail: msur@mit.edu

inputs, or do they show similar tuning and maps as do their neighboring neurons? Is the spatial resolution of astrocyte activation sufficient to support hemodynamic mapping methods? If so, what influence do astrocytes have on hemodynamic mapping signals? We addressed these issues by performing parallel two-photon calcium imaging of neurons and astrocytes and optical imaging of blood-volume changes in a single, well-characterized model system. We investigated the visual tuning and mapping of astrocytes, along with their influence on hemodynamic signals and neuronal responses, in the primary visual cortex (V1) of ferrets by loading cells with the fluorescent calcium indicator Oregon Green Bapta (OGB1) (*25*, *26*) and the specific astrocytic marker sulforhodamine101 (SR101) (*20*) and using two-photon imaging to simultaneously monitor the visual activity of neurons and that of neighboring astrocytes (*27*) (movie S1).

Our first finding is that astrocytes in the visual cortex respond to visual stimuli with robust increases in calcium concentration. Fig. 1A (left panel) shows double labeling of a 50-by-50–μm square patch of cortex, 120 μm below the pial surface containing neurons and an astrocyte. Fig. 1B shows the responses of the two cells circled in Fig. 1A to a visual stimulus consisting of a drifting grating. The neuron (blue trace) shows a fluorescence increase of close to 10%, which begins at the time of stimulus onset and lasts throughout the duration of the stimulus presentation. The astrocyte response (red trace) also exhibits a stimulus-locked calcium increase, which is delayed roughly 3 to 4 s from stimulus onset (movie S2). Whereas calcium increases in neurons result from spiking activity (*28*, *29*), astrocyte responses are attributable to a delayed release of calcium from internal stores (*30*). The existence of visually evoked calcium responses in astrocytes led us to ask whether astrocytes have spatially restricted receptive fields, similar to those found in neurons in the visual cortex. We tested the spatial extent of stimuli eliciting astrocyte responses by presenting vertical or horizontal bars moving sequentially across visual space. Astrocytes responded to stimuli over a similar region of space as neighboring neurons (Fig. 1C). Both the location of maximal response and the extent of the receptive field were comparable in the *x* and *y* dimensions of space. Contour plots of responses show that nearby neurons and astrocytes have largely overlapping receptive fields (Fig. 1D).

We next examined whether astrocytes have other receptive-field characteristics found in neurons. We first tested orientation tuning with drifting gratings of different orientations. Fig. 1E shows plots of the responses of an astrocyte and a neuron to the presentation of drifting gratings of six orientations, spanning 180° at 30° intervals. The neuron (blue trace in Fig. 1E, middle panels) shows a visual response to a narrow range of orientations, as was expected from previous studies using calcium imaging or direct measurement of firing rate (*24*, *31*, *32*). The tuning curve (below) is typical of neurons in ferret V1 (*33*, *34*). The astrocyte (red trace) also has clear orientation tuning (Fig. 1E, right panels). Furthermore, the preferred orientation of the astrocyte is very

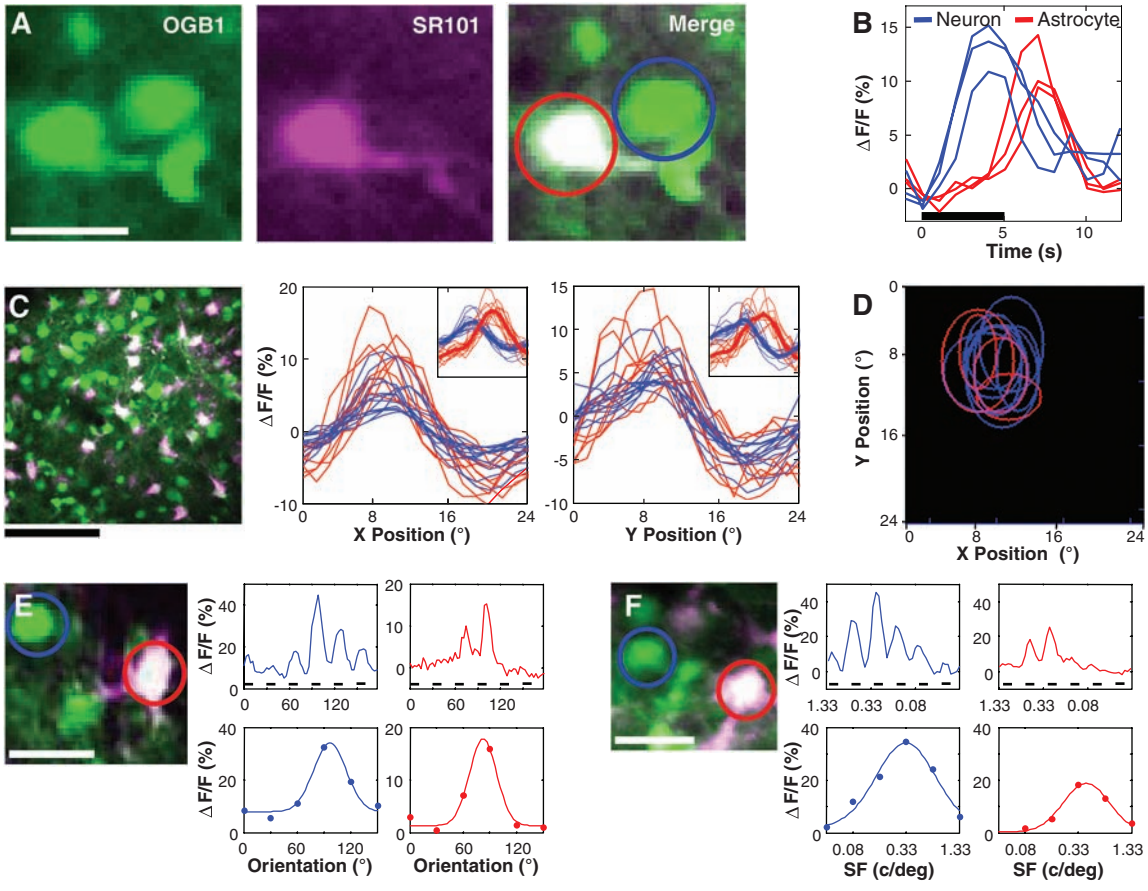

Fig. 1. Astrocytes have robust visual responses, spatially restricted receptive fields, and stimulus-feature selectivity. (**A**) Double labeling of a patch of cortex 120 μm below the pial surface. From left to right, the panels show cells loaded with the calcium indicator OGB1, astrocyte marker SR101, and merged OGB1 and SR101. Scale bar, 25 μm. (**B**) Time course of visually evoked responses (Δ*F*/*F*) in the neuron (blue) and astrocyte (red) outlined in the right panel of (A). The stimulus consists of three trials of a drifting grating presented for 5 s (indicated by the thick black bar). (**C**) Measurements of receptive-field location and extent in a population of neurons and astrocytes, labeled green and purple, respectively, in the merged image at left. Responses of neurons (blue) and astrocytes (red) to vertical (center panel) and horizontal (right panel) bars swept periodically across the receptive field. Each trace plots the cycle-averaged response for one cell. Scale bar, 100 μm. (Insets) Raw responses as a function of time, before aligning the astrocyte and neuron responses by subtracting a constant delay from the astrocyte responses. (Insets) *x* axis, time (0 to 18 s); *y* axis, Δ*F*/*F* (–10 to 20%). (**D**) Contour plots of the half-maximal response to *x* and *y* bars for a subset of neurons and astrocytes. Receptive fields of astrocytes are indicated in red; those of neurons are shown in blue. (**E**) Responses of a neuron (blue circle) and an astrocyte (red circle) to drifting gratings of varying orientation. Scale bar, 25 μm. (Right) Top panels show the responses to six orientations evenly spaced between 0° and 180° as a function of time, as orientation is systematically changed. Stimuli lasting 5 s (dashed lines) are alternated with 5-s blank periods. Bottom panels show the tuning curves computed from the responses above and the Gaussian fits to the curves. (**F**) Responses of a neuron and an astrocyte (both circled in left panel) to gratings of varying spatial frequency. Scale bar, 25 μm. (Right) Responses, in a format similar to that in (E). Spatial frequencies were presented in decreasing order, from 1.33 to 0.04 cycles per degree. Tuning curves were fit with a Gaussian function and are plotted as a function of increasing spatial frequency.

similar to that of the nearby neuron, suggesting that there may be spatial alignment of orientation preference between neurons and astrocytes. We also measured the responses of astrocytes to gratings varying in spatial frequency. The neuron in Fig. 1F (middle panels) shows spatial-frequency tuning typical of visual cortical neurons in ferret V1 (*35*). The astrocyte is also selective for spatial frequency (Fig. 1F, right panels).

We then analyzed the tuning characteristics of astrocytes in more detail. We made OGB1 injections into orientation domains, thus labeling a population of cells with a relatively homogeneous orientation preference, and subsequently obtained high-resolution tuning curves with stimulus sampling at 10° intervals. Astrocytes were even more sharply tuned for orientation than neurons (Fig. 2A). On average, neurons responded to a stimulus 20° from the preferred—roughly half as much as to the preferred orientation—whereas astrocytes responded only minimally, if at all. We fitted the tuning curves [calculated from fractional change in fluorescence (F); $\Delta F/F$] with a Gaussian function to quantify differences in tuning. There was a significant difference in tuning width, which is apparent in the overlaid tuning curves (Fig. 2B)

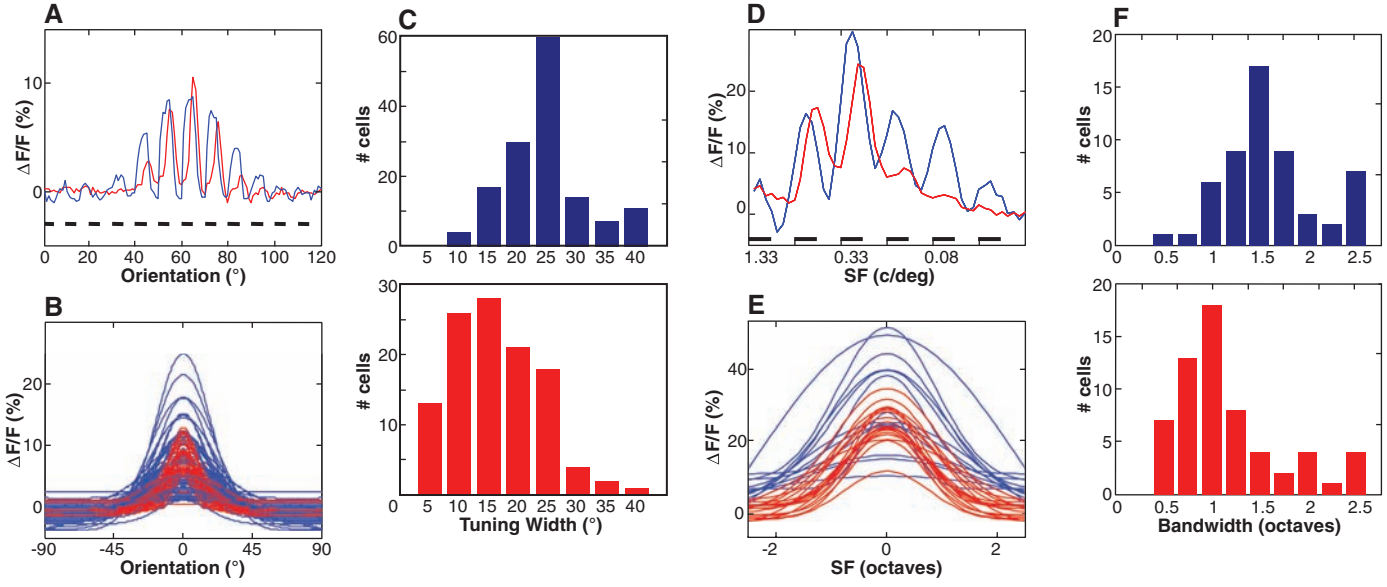

Fig. 2. Astrocytes have sharper orientation and spatial-frequency tuning than neurons. (**A**) Average stimulus-evoked response of a population of neurons (blue, n = 80 neurons) and astrocytes (red, n = 69 astrocytes) from the same regions of the visual cortex to gratings of different orientations. The response of each cell was aligned to its preferred orientation before averaging. The stimulus presentation time for each orientation is indicated by the short black horizontal bars; the display was blank in the intervening intervals. (**B**) Overlaid Gaussian fits to the tuning curves of all neurons (blue, n = 80) and astrocytes (red, n = 69). (**C**) Population histograms of the orientation tuning width, measured as half width at half height, pooled from three ferrets. Top, neurons (n = 143); bottom, astrocytes (n = 113). (**D**) Average stimulus-evoked response of a population of adjacent neurons (blue, n = 13) and astrocytes (red, n = 17) to gratings of varying spatial frequency. The stimulus presentation time for each spatial frequency is indicated by the black horizontal bars; the display was blank in the intervening intervals. (**E**) Overlaid Gaussian fits to the tuning curves of all neurons (blue, n = 13) and astrocytes (red, n = 17). (**F**) Population histograms of the spatial-frequency tuning width, measured as half width at half height, pooled from three ferrets. Top, neurons (n = 49); bottom, astrocytes (n = 47).

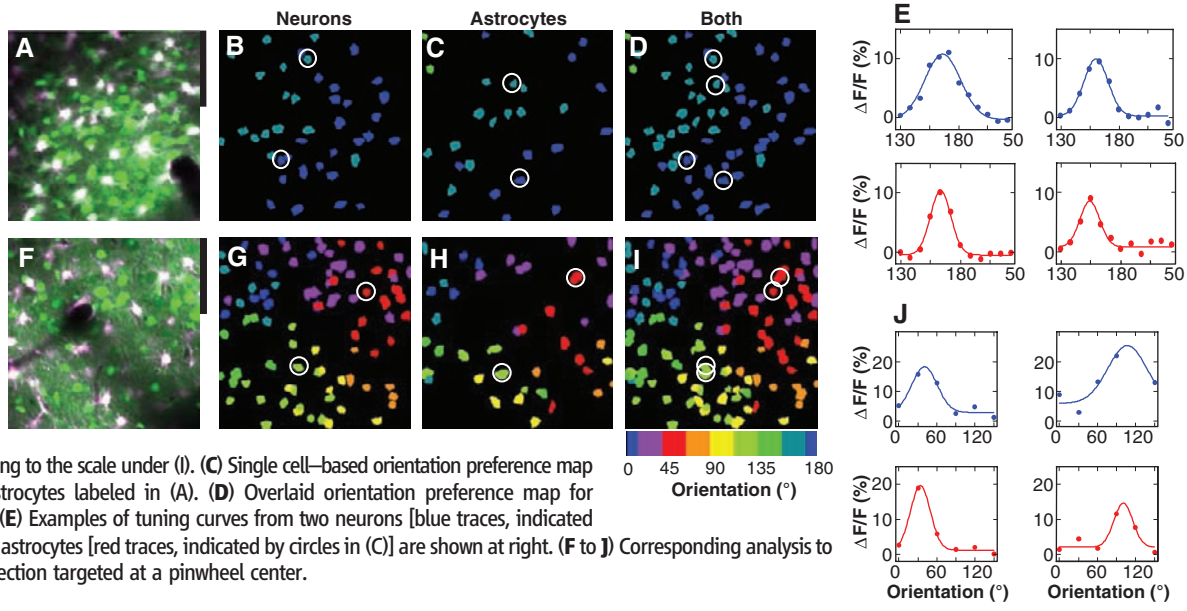

Fig. 3. Astrocyte- and neuronal-orientation preference is mapped precisely across the cortical surface. (**A**) Merged image of SR101 and OGB1 label in a 250-by-250–μm patch of cortex 120 μm below the pial surface. (**B**) Single cell–based orientation preference map for the population of neurons labeled in (A). Orientation preference was determined by Gaussian fits to the data and is coded according to the scale under (I). (**C**) Single cell–based orientation preference map for the population of astrocytes labeled in (A). (**D**) Overlaid orientation preference map for neurons and astrocytes. (**E**) Examples of tuning curves from two neurons [blue traces, indicated by circles in (B)] and two astrocytes [red traces, indicated by circles in (C)] are shown at right. (**F** to **J**) Corresponding analysis to (A to E) for a second injection targeted at a pinwheel center.

and in the histograms of half width at half height (Fig. 2C; mean tuning width of neurons, 24.9°; n = 143 cells from three ferrets; mean tuning width of astrocytes, 16.4°; n = 113 cells from three ferrets; $P < 0.01$; t test).

Next, we quantitatively examined the tuning of astrocyte responses to spatial frequency and compared them with adjacent neurons. Astrocytes were more sharply tuned for spatial frequency than neurons (Fig. 2, D to F). On average, neurons responded to a much broader range of spatial frequencies, especially in the lower frequency range. The tuning bandwidth of astrocytes (0.8 octaves) was significantly narrower than that of neurons (1.5 octaves, $P < 0.01$, t test, n = 49 neurons, 47 astrocytes from three ferrets). Furthermore, the preferred response features tended to be clustered, such that groups of nearby neurons and astrocytes have similar preferred orientations (see also below) and spatial frequencies (fig. S1), though with a range of tuning widths.

Neuronal receptive-field tuning preferences are organized into two-dimensional maps across V1 (*36*–*40*). We thus asked if the receptive-field properties of astrocytes are organized in a similar manner. Two-photon imaging is well suited to the mapping of cellular activity at single-cell resolution (*24*, *25*, *32*). We could therefore simultaneously image the spatial arrangement of neuronal and astrocytic orientation tuning over 250-by-250–μm expanses of the cortex (Fig. 3A). We first analyzed the cellular organization of tuning in an orientation domain, where there is a relatively uniform neuronal preferred orientation. An orientation map of individ-

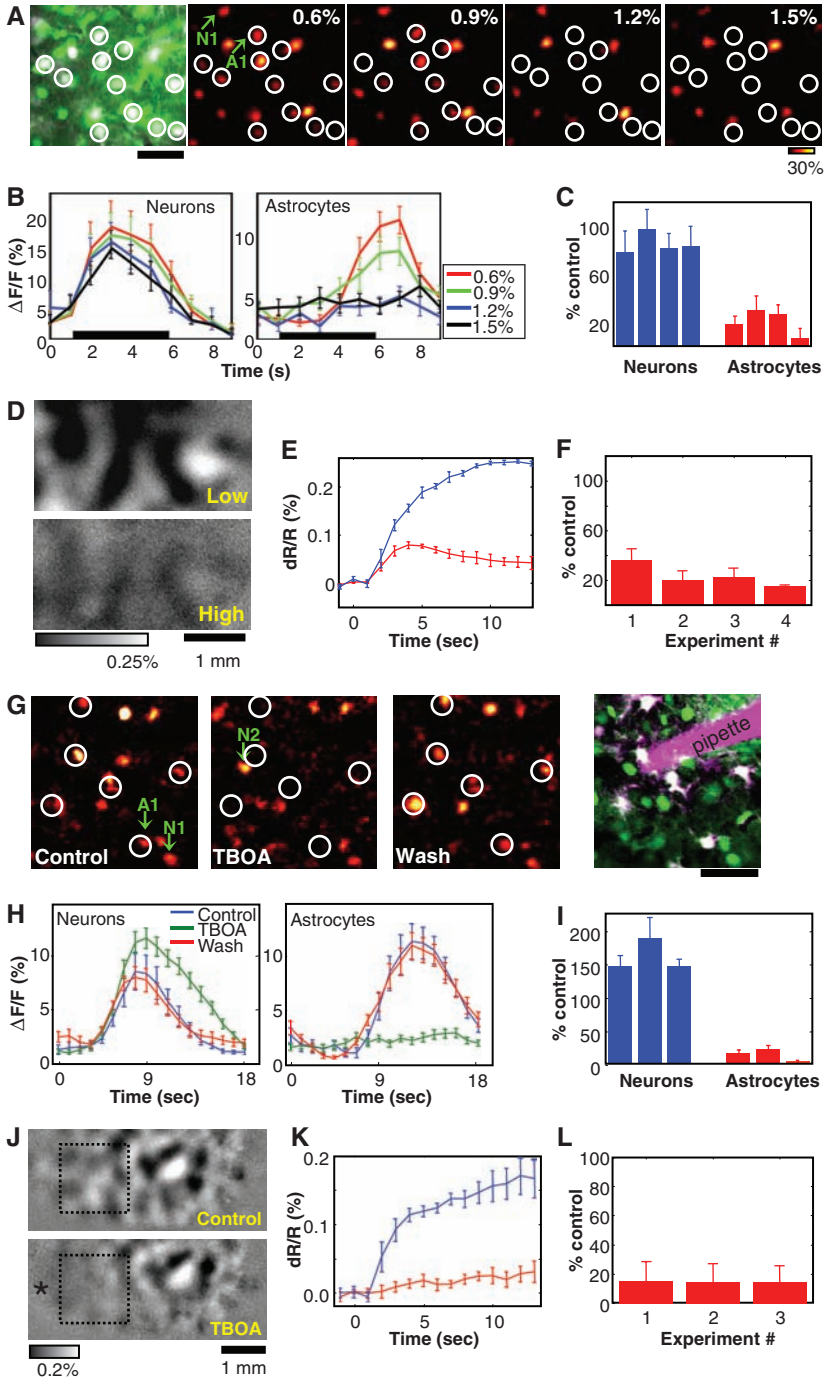

Fig. 4. Astrocyte calcium responses and the intrinsic optical signal are selectively affected by specific blockers. (**A**) Dose-dependant effect of isoflurane on the responses of neurons and astrocytes. The response amplitude of a field of neurons and astrocytes at different isoflurane levels (0.6, 0.9, 1.2, and 1.5%) is shown. White circles indicate astrocytes, and arrows indicate a representative neuron (N1) and astrocyte (A1) whose time course of visual responses under different isoflurane levels is shown in fig. S5. Scale bar, 50 μm. (**B**) Mean response time courses of the neurons (n = 8) and astrocytes (n = 11) from the field of view in (A). Stimulus time is indicated by the black bar. (**C**) Average neuron and astrocyte response suppression by high isoflurane (n = 33 neurons from four ferrets and 44 astrocytes from four ferrets). Each bar shows data from a single animal and depicts the response level under high isoflurane relative to low. (**D**) Example of intrinsic-signal optical imaging differential (0° – 90°) maps, computed from 4 to 13 s, during low- and high-isoflurane conditions. (**E**) Plots of the time course of reflectance change (dR/R, where R is reflectance) (mean ± SEM, indicated by error bars) in the example shown in (D). Stimulus was turned on at time 0 s. Blue line, low isoflurane; red line, high isoflurane. Each line shows the average ± SEM of five traces under each condition. (**F**) Summary of mapping-signal suppression by high isoflurane from four ferrets. Each bar shows data from a single animal. (**G**) Magnitude map for visually driven responses in a field of cells before, during, and after application of the glutamate transporter antagonist TBOA. Astrocytes are circled in white. The position of the TBOA pipette and dual labeling of astrocytes (white) and neurons (green) are shown in far right panel. Arrows mark an astrocyte (A1) and two neurons (N1 and N2) whose time course of visual responses before, during, and after TBOA application is shown in fig. S6. Scale bar, 50 μm. (**H**) Mean (± SEM, indicated by error bars) responses of a population of 13 astrocytes and 25 neurons from the same experiment as in (G) [(G) shows a zoomed-in portion of the entire imaged region] to a continuously changing orientation stimulus before, during, and after TBOA application. The response duration is prolonged during TBOA application. (**I**) Summary bar plot of the effect of TBOA on astrocyte and neuron responses from three experiments (67 neurons and 32 astrocytes from three ferrets). Each bar shows data from a single animal. (**J**) Differential intrinsic-signal maps (0° – 90°) before and during TBOA application. TBOA was applied from a cannula positioned at the asterisk. Dotted boxes indicate the portion of the map used to calculate the time course of the mapping signal in (K). (**K**) Time course of the mapping-signal magnitude (mean ± SEM, indicated by error bars), calculated from the portion of the map indicated by the rectangle in the top panel of (J). (**L**) Summary bar plot of the mean (± SEM, indicated by error bars) suppression of the mapping signal by TBOA from three ferrets. Each bar shows data from a single animal. Error bars throughout the figure indicate SEM.

ual cells demonstrates that the spatial organization of neuronal-orientation preference (Fig. 3B) and the organization of orientation preference in the interposed population of astrocytes (Fig. 3C) closely match each other (Fig. 3D). Examples of $\Delta F/F$ tuning curves of two neurons and two astrocytes are plotted in Fig. 3E. Quantitative analysis of the rate of change and scatter demonstrates that the spatial organization of astrocyte and neuron orientation tuning was indistinguishable within an orientation domain (fig. S2).

Orientation tuning of neurons in V1 is organized with high precision, at the level of individual neurons (*24*). We were interested to know whether the preferred orientation of astrocytes has a similar degree of organization. To further test the spatial resolution of astrocyte-orientation mapping, we made injections of OGB1 in pinwheel centers and orientation fractures, which are locations in the orientation map where preferred orientation changes dramatically on a short spatial scale (<50 μm). The single cell–based neuron maps closely match orientation maps obtained with optical imaging of intrinsic signals (fig. S3). The example in Fig. 3, F to J, demonstrates that the astrocyte-orientation map was just as precise as that of neurons. The single cell–based orientation map of neurons is shown in Fig. 3G (movie S3). The pinwheel center was remarkably distinct; there was no overlap of orientation preferences across the pinwheel center. The same holds true for astrocytes (Fig. 3H). The overlay of the two maps (Fig. 3I) shows that the alignment of the pinwheel center was matched perfectly. Quantitative analyses demonstrate that the orientation preference of astrocyte responses was mapped just as precisely as that of neuronal responses (fig. S2). Thus, there is a remarkable degree of specificity in the mechanisms responsible for generating and mapping orientation tuning in astrocytes. This is particularly notable, given that the presynaptic activity in the neuropil surrounding a pinwheel is very poorly tuned (fig. S4). In contrast to some situations in vitro where astrocyte activity has been associated with "calcium waves" that propagate through large networks of interconnected cells (*41*), our data demonstrate that, in vivo, astrocytes behave relatively independently of each other: Each astrocyte is sharply tuned for orientation, and two astrocytes only tens of microns apart can respond to orthogonal stimulus orientations.

The sharp tuning of astrocytes suggests the possibility that a high level of local neuronal activity is necessary to elicit astrocyte responses. In support of this hypothesis, we found that small changes in isoflurane concentration, over a narrow range of concentrations around ~1%, produce a modest reduction of neuronal responses but a dramatic reduction of astrocyte responses (Fig. 4, A to C). Fig. 4A shows the magnitude map for a field of neurons and astrocytes at different concentrations of isoflurane. The responses of astrocytes (circled in white) were reduced in a dose-dependent manner, with a sharp fall-off between 0.9 and 1.2% (fig. S5). The average reduction in astrocyte responses under high isoflurane (>1%) compared with low (<1%) was 77 ± 14% (44 astrocytes from four ferrets, $P < 0.001$ comparing individual animals, *t* test), whereas neuronal responses were only reduced by 16 ± 8% (33 neurons from four ferrets, $P < 0.001$, *t* test) (Fig. 4C).

We have taken advantage of the differential sensitivity of astrocytes and neurons to isoflurane to directly probe the role of astrocytes in translating neuronal-orientation maps into hemodynamic maps. Astrocyte activity leads to vasodilation in vitro (*14*, *16*, *42*, *43*) and in vivo (*15*, *16*). However, the spatial scale of astrocyte-mediated neurovascular coupling is unknown, and this is a critical factor for functional imaging of orientation maps. Spatial blurring of hemodynamic signals would lead to systematic errors of optically imaged orientation maps (*44*), whereas we find that the optical map matches the neuronal map nearly perfectly (fig. S3). To address the role of astrocytes in the ability to image high-resolution orientation maps with intrinsic signals, we performed optical imaging under identical conditions as our two-photon experiments. We used green (546-nm) light, which emphasizes changes in blood volume (*45*), and measured the mapping signal from orthogonal stimulus orientations. Concentrations of isoflurane that preferentially reduce astrocyte responses led to a large reduction in the differential orientation maps, with an average mapping-signal reduction of 77 ± 9% (Fig. 4, D to F; four ferrets; $P < 0.001$; *t* test). Thus, the ability to reliably measure the pinwheel structure of orientation maps with hemodynamic imaging (fig. S3) is probably due to the highly localized engagement of astrocytes by neuronal activity.

One potential concern about these results is that neuronal activity is also reduced, though modestly, by isoflurane, which could possibly lead to direct reduction of the blood-volume response (*46*–*48*). We therefore sought a means to block astrocytic responses without interfering with neuronal synaptic transmission. One mechanism to trigger astrocyte responses is the activation of glutamate transporters (*49*, *50*). Astrocyte glutamate transporters provide the major mechanism for glutamate clearance from the synaptic cleft, and their activity tightly regulates the amplitude and kinetics of synaptic transmission in vitro (*51*). Fig. 4G shows the response magnitudes of a field of neurons and astrocytes before, during, and after application of the glutamate transporter antagonist DL-threo-β-benzyloxyaspartate (TBOA) via a visualized pipette. The responses of astrocytes (circled in white) were clearly and significantly reduced (Fig. 4, H and I; 88 ± 10% reduction; 32 astrocytes from three ferrets; $P < 0.001$; *t* test). The responses of neurons were increased to a lesser extent (58 ± 25% increase, 67 neurons from three ferrets, $P < 0.001$, *t* test), and some neurons that were unresponsive in the control condition became measurably responsive during TBOA application (Fig. 4G and fig. S6). Furthermore, neuronal responses were prolonged during TBOA application (Fig. 4H), consistent with an increase in glutamate availability at synapses because it is not cleared by astrocyte transporters. These data demonstrate a key role for astrocytes in regulating the strength and time course of neuronal responses to incoming synaptic inputs.

Having demonstrated that TBOA is an effective means to silence astrocytes without any potential confound from reducing neuronal responses, we next tested the effects of TBOA on stimulus-specific blood-volume responses with optical imaging. TBOA reduced these signals to <20% of control (n = three ferrets; $P < 0.001$; *t* test; Fig. 4, J to L)—a notable effect, given that neuronal responses are actually increased during TBOA application. The orientation-selective mapping signals from intrinsic-signal imaging were reduced to a similar extent as those of the astrocyte calcium responses (by 85 ± 2%; mean of three ferrets; Fig. 4L).

We have demonstrated the visual response properties and detailed organization of astrocytes in the visual cortex. Astrocytes exhibit robust calcium responses to visual stimuli that are dependent on stimulus features and have many of the receptive-field characteristics of neurons. In particular, they have well-defined spatial receptive fields, orientation tuning, and spatial-frequency tuning. What's more, astrocytes are more sharply tuned for orientation and spatial frequency than neurons. Additionally, the orientation preference of astrocytes is exquisitely mapped across the cortex at single-cell resolution, in close register with the neuronal-orientation preference map. This suggests that, in vivo, astrocytes do not necessarily function as a broadly interconnected network [as has been suggested by some in vitro studies (*41*, *52*)], but rather that each astrocyte interacts quasi-independently with a small number of neurons surrounding it. Future work will be necessary to determine whether groups of astrocytes with similar response properties form distinct syncytia. Furthermore, astrocyte calcium responses are a critical step in local hemodynamic regulation, as is commonly measured with intrinsic-signal optical imaging and blood oxygen level–dependent functional magnetic resonance imaging.

Our findings indicate that the spatial scale of synaptic interactions between neurons and astrocytes is extremely precise. In orientation domains, where the presynaptic inputs are highly orientation selective (fig. S4) (*22*, *23*), it is not surprising that astrocytes and neurons have similar orientation tuning. However, at orientation pinwheels, where the inputs are almost untuned (fig. S4) (*22*, *23*) but neurons are sharply tuned because of a combination of the spike threshold and balanced inhibition (*23*), astrocytes surprisingly have similar orientation preference

as their neighboring neurons, and their tuning is even sharper. There are several potential explanations for the sharp tuning of astrocyte responses. Astrocyte visual responses probably arise from the presynaptic activity of afferent and/or recurrent inputs at synapses with closely abutting astrocytic processes. An important basis for astrocyte calcium responses in the ferret visual cortex is the binding of glutamate to astrocyte glutamate transporters. Though the signaling pathway is not fully known, it is feasible that the depolarization caused by the transporter current triggers calcium influx in astrocytes via voltage-dependent calcium channels or by the release of calcium from intracellular stores (*53*). It is possible that threshold levels of presynaptic activity need to be crossed to activate glutamate transporters on astrocytes; such a threshold could, in principle, account for sharper astrocyte tuning. Our data showing that increased isoflurane leads to small decreases in neuronal responses but large decreases in astrocyte responses supports this hypothesis. However, alternative interpretations are also possible. Astrocytes may sample presynaptic activity over a smaller spatial scale than neurons (and thus from a smaller region within a feature map), leading to sharper tuning. It is also possible that astrocytes may not sample uniformly from synapses within their anatomical span. If they had a higher proportion of processes or a higher density of receptors/transporters at the strongest synapses, this could effectively increase their response selectivity. Regardless of the mechanism, however, the sharp response tuning of astrocytes and their precise mapping, combined with their highly selective vascular effects, probably contributes critically to the ability of hemodynamic imaging methods to obtain valid measures of neuronal activity.

It is worth noting that the functional contribution of astrocytes includes the regulation of neuronal response magnitude and duration. In vitro studies demonstrate that astrocytes release glutamate upon activation (*7*–*10*), are closely apposed structurally to spines (*4*, *5*), and influence synaptic strength between neurons (*10*, *12*, *13*). This suggests that they may also influence temporal dynamics of neuronal responses during adaptation or learning in vivo (*54*–*56*).

References and Notes

1. M. Nedergaard, B. Ransom, S. A. Goldman, *Trends Neurosci.* **26**, 523 (2003).
2. R. D. Fields, B. Stevens-Graham, *Science* **298**, 556 (2002).
3. A. Volterra, J. Meldolesi, *Nat. Rev. Neurosci.* **6**, 626 (2005).
4. M. Haber, L. Zhou, K. K. Murai, *J. Neurosci.* **26**, 8881 (2006).
5. R. Ventura, K. M. Harris, *J. Neurosci.* **19**, 6897 (1999).
6. J. T. Porter, K. D. McCarthy, *J. Neurosci.* **16**, 5073 (1996).
7. A. Araque, N. Li, R. T. Doyle, P. G. Haydon, *J. Neurosci.* **20**, 666 (2000).
8. L. Hertz, H. R. Zielke, *Trends Neurosci.* **27**, 735 (2004).
9. V. Montana, Y. Ni, V. Sunjara, X. Hua, V. Parpura, *J. Neurosci.* **24**, 2633 (2004).
10. J. M. Zhang *et al.*, *Neuron* **40**, 971 (2003).
11. E. A. Newman, *Trends Neurosci.* **26**, 536 (2003).
12. J. Kang, L. Jiang, S. A. Goldman, M. Nedergaard, *Nat. Neurosci.* **1**, 683 (1998).
13. N. Kang, J. Xu, Q. Xu, M. Nedergaard, J. Kang, *J. Neurophysiol.* **94**, 4121 (2005).
14. S. J. Mulligan, B. A. MacVicar, *Nature* **431**, 195 (2004).
15. T. Takano *et al.*, *Nat. Neurosci.* **9**, 260 (2006).
16. M. Zonta *et al.*, *Nat. Neurosci.* **6**, 43 (2003).
17. D. R. Harder, N. J. Alkayed, A. R. Lange, D. Gebremedhin, R. J. Roman, *Stroke* **29**, 229 (1998).
18. P. G. Haydon, G. Carmignoto, *Physiol. Rev.* **86**, 1009 (2006).
19. H. Hirase, L. Qian, P. Bartho, G. Buzsaki, *PLoS Biol.* **2**, E96 (2004).
20. A. Nimmerjahn, F. Kirchhoff, J. N. Kerr, F. Helmchen, *Nat. Methods* **1**, 31 (2004).
21. X. Wang *et al.*, *Nat. Neurosci.* **9**, 816 (2006).
22. J. Schummers, J. Mariño, M. Sur, *Neuron* **36**, 969 (2002).
23. J. Mariño *et al.*, *Nat. Neurosci.* **8**, 194 (2005).
24. K. Ohki *et al.*, *Nature* **442**, 925 (2006).
25. F. Helmchen, W. Denk, *Nat. Methods* **2**, 932 (2005).
26. C. Stosiek, O. Garaschuk, K. Holthoff, A. Konnerth, *Proc. Natl. Acad. Sci. U.S.A.* **100**, 7319 (2003).
27. Materials and methods are available as supporting material on *Science* Online.
28. J. N. Kerr, D. Greenberg, F. Helmchen, *Proc. Natl. Acad. Sci. U.S.A.* **102**, 14063 (2005).
29. D. Smetters, A. Majewska, R. Yuste, *Methods* **18**, 215 (1999).
30. G. Perea, A. Araque, *J. Neurosci.* **25**, 2192 (2005).
31. D. H. Hubel, T. N. Wiesel, *J. Physiol.* **160**, 106 (1962).
32. K. Ohki, S. Chung, Y. H. Ch'ng, P. Kara, R. C. Reid, *Nature* **433**, 597 (2005).
33. H. J. Alitto, W. M. Usrey, *J. Neurophysiol.* **91**, 2797 (2004).
34. B. Chapman, M. P. Stryker, *J. Neurosci.* **13**, 5251 (1993).
35. G. E. Baker, I. D. Thompson, K. Krug, D. Smyth, D. J. Tolhurst, *Eur. J. Neurosci.* **10**, 2657 (1998).
36. A. Basole, L. E. White, D. Fitzpatrick, *Nature* **423**, 986 (2003).
37. T. Bonhoeffer, A. Grinvald, *Nature* **353**, 429 (1991).
38. M. Hubener, D. Shoham, A. Grinvald, T. Bonhoeffer, *J. Neurosci.* **17**, 9270 (1997).
39. N. P. Issa, C. Trepel, M. P. Stryker, *J. Neurosci.* **20**, 8504 (2000).
40. H. Yu, B. J. Farley, D. Z. Jin, M. Sur, *Neuron* **47**, 267 (2005).
41. A. H. Cornell-Bell, S. M. Finkbeiner, M. S. Cooper, S. J. Smith, *Science* **247**, 470 (1990).
42. J. A. Filosa, A. D. Bonev, M. T. Nelson, *Circ. Res.* **95**, e73 (2004).
43. M. R. Metea, E. A. Newman, *J. Neurosci.* **26**, 2862 (2006).
44. J. R. Polimeni, D. Granquist-Fraser, R. J. Wood, E. L. Schwartz, *Proc. Natl. Acad. Sci. U.S.A.* **102**, 4158 (2005).
45. R. D. Frostig, E. E. Lieke, D. Y. Ts'o, A. Grinvald, *Proc. Natl. Acad. Sci. U.S.A.* **87**, 6082 (1990).
46. D. Attwell, C. Iadecola, *Trends Neurosci.* **25**, 621 (2002).
47. B. Cauli *et al.*, *J. Neurosci.* **24**, 8940 (2004).
48. A. Rancillac *et al.*, *J. Neurosci.* **26**, 6997 (2006).
49. D. De Saint Jan, G. L. Westbrook, *J. Neurosci.* **25**, 2917 (2005).
50. H. Gurden, N. Uchida, Z. F. Mainen, *Neuron* **52**, 335 (2006).
51. C. M. Anderson, R. A. Swanson, *Glia* **32**, 1 (2000).
52. J. W. Dani, A. Chernjavsky, S. J. Smith, *Neuron* **8**, 429 (1992).
53. A. Verkhratsky, R. K. Orkand, H. Kettenmann, *Physiol. Rev.* **78**, 99 (1998).
54. V. Dragoi, C. Rivadulla, M. Sur, *Nature* **411**, 80 (2001).
55. T. O. Sharpee *et al.*, *Nature* **439**, 936 (2006).
56. J. Schummers, J. Sharma, M. Sur, *Prog. Brain Res.* **149**, 65 (2005).

57. We thank A. Majewska for initial and ongoing assistance with two-photon microscopy and helpful comments on a draft of the paper. This work was supported by grants from the NIH and the Simons Foundation (to M.S.).

Supporting Online Material

www.sciencemag.org/cgi/content/full/320/5883/1638/DC1
Materials and Methods
Figs. S1 to S6
Movies S1 to S3

5 February 2008; accepted 25 April 2008
10.1126/science.1156120

Proliferating Cells Express mRNAs with Shortened 3′ Untranslated Regions and Fewer MicroRNA Target Sites

Rickard Sandberg,[1]*† Joel R. Neilson,[2]* Arup Sarma,[3] Phillip A. Sharp,[1,2]‡ Christopher B. Burge[1]‡

Messenger RNA (mRNA) stability, localization, and translation are largely determined by sequences in the 3′ untranslated region (3′UTR). We found a conserved increase in expression of mRNAs terminating at upstream polyadenylation sites after activation of primary murine CD4$^+$ T lymphocytes. This program, resulting in shorter 3′UTRs, is a characteristic of gene expression during immune cell activation and correlates with proliferation across diverse cell types and tissues. Forced expression of full-length 3′UTRs conferred reduced protein expression. In some cases the reduction in protein expression could be reversed by deletion of predicted microRNA target sites in the variably included region. Our data indicate that gene expression is coordinately regulated, such that states of increased proliferation are associated with widespread reductions in the 3′UTR-based regulatory capacity of mRNAs.

The 3′ untranslated region (3′UTR) of mRNA has known functions in the stability, localization, and translation of mRNA (*1*). These roles are mediated by interactions with regulatory proteins and RNAs, including microRNAs (miRNAs) (*2*). About half of mammalian genes use alternative cleavage and polyadenylation (APA) to generate multiple mRNA isoforms differing in their 3′UTRs (*3*–*5*). However, the extent to which differential expression of these isoforms is used to regulate mRNA and protein levels in cellular proliferation and differentiation programs is poorly understood.

T lymphocyte activation is central to the immune response, and much is known about the associated gene expression and regulation (*6*).

[1]Department of Biology, Massachusetts Institute of Technology, Cambridge, MA 02139, USA. [2]Koch Institute for Integrative Cancer Research, Massachusetts Institute of Technology, Cambridge, MA 02139, USA. [3]Department of Electrical Engineering and Computer Science, Massachusetts Institute of Technology, Cambridge, MA 02139, USA.

*These authors contributed equally to this work.
†Present address: Department of Cell and Molecular Biology, Karolinska Institutet, 171 77 Stockholm, Sweden.
‡To whom correspondence should be addressed. E-mail: sharppa@mit.edu (P.A.S.); cburge@mit.edu (C.B.B.)